

NANO EXPRESS

Open Access



# Time-Resolved Luminescence Properties of Laser-Fabricated Nano-diamonds

Juan Hao<sup>1</sup>, Lingyun Pan<sup>2\*</sup>, Minghui An<sup>1</sup>, Yunzhi Dai<sup>1</sup> and Bingrong Gao<sup>1\*</sup>

## Abstract

In the study, well-crystallized nano-diamonds with an average size of 3.8 nm are obtained via femtosecond laser ablation. Both steady-state and transient luminescence are observed. The luminescence peaks of nano-diamonds shift from 380 to 495 nm when the excitation wavelength changes from 280 to 420 nm. After passivation by polyethylene glycol-400N, the surface of nano-diamonds is significantly oxidized, which is verified by Raman and UV-Vis absorption spectra. Furthermore, there is no change in all the luminescence wavelengths, although the maximum intensity increases by 10 times. Time-resolved luminescence spectra reveal that trapping states can be modified by surface passivation, and this leads to stronger luminescence with a longer lifetime.

**Keywords:** Nano-diamonds, Pulsed laser ablation, Luminescence, Surface modification

## Introduction

Carbon nanomaterials including quantum dots, nanowires, and thin films play an important role in the application of novel materials [1–6]. When compared with other carbon nanomaterials, nano-diamonds (NDs) exhibit unique advantages and applications in the electronics industry, genetic engineering, pharmaceutical engineering, and lithium-ion batteries [7, 8]. Zimmermann et al. demonstrated that heterostructure diodes built using ultra-small NDs exhibit high performance in the ultraviolet region as well as in terms of rectification and temperature stability at 1050 °C [9]. Wang et al. examined the delivery of epirubicin using NDs 2–20 nm in diameter, and this is expected to overcome chemoresistance in cancer stem cells and improve the therapeutic effect in hepatic cancers [10]. Ho et al. revealed that NDs only 2–5 nm in size can achieve gene delivery by entering the nucleus via passive transport [11]. Additionally, it shows that the performance of the battery can be significantly improved by adding NDs (< 5 nm) to the electrolytic cell of a lithium battery, and the effect is

more positive with decreases in size [12]. Thus, it is imperative to produce NDs less than 5 nm in size.

However, it is difficult to fabricate uniformly distributed 5-nm NDs via conventional methods. Currently, the main method for preparing NDs is through a high temperature and pressure explosion. The size of NDs obtained by this method is about 4 nm, but the stand-by size always exceeds 100 nm due to agglomeration [13]. Although various de-agglomeration methods have been explored, even the best method can only disintegrate the large agglomerated particles to approximately 10 nm [14]. Extant studies continue to explore well-dispersed and ultra-small (< 5 nm) NDs and significantly more green, simple, and ambient methods. Sankaran et al. fabricated NDs in the range of 2–5 nm via microplasma dissociation of ethanol vapor [15]. However, ND chains are formed due to agglomeration [16]. Tan et al. successfully obtained well-dispersed NDs of 2–4 nm via femtosecond pulsed laser ablation in liquid (fs-PLAL) [17]. However, the conversion efficiency of graphite or carbon materials to diamond through ablation is excessively low to improve the yield of NDs [17–19].

Given the development of preparation technology, there is a gradual increase in studies on the optical properties of NDs. Shenderova et al. concluded that NDs include a series of luminescence centers from blue to red

\* Correspondence: [ply@jlu.edu.cn](mailto:ply@jlu.edu.cn); [brgao@jlu.edu.cn](mailto:brgao@jlu.edu.cn)

<sup>2</sup>College of Physics, Jilin University, Changchun 130012, People's Republic of China

<sup>1</sup>College of Electronic Science and Engineering, Jilin University, Changchun 130012, People's Republic of China

[20]. Schmidt et al. realized energy transfer and manipulation of the molecular chain via utilizing fluorescent NDs [21]. Furthermore, many biological applications were realized based on the luminescence properties of NDs via surface modification [22, 23]. Therefore, it is necessary to investigate their luminescence properties. In particular, luminescence dynamics constitutes helpful data to understand the mechanisms of emission process, and there is a paucity of studies examining the same.

In the study, we used fs-PLAL on bulk diamond in ethanol. As a result, a large amount of well-dispersed NDs with 3.8 nm average size and naked surface were successfully obtained. The NDs were then passivated by bio-compatible polyethylene glycol-400N (PEG<sub>400N</sub>). Both steady-state and transient luminescence of un-passivated and passivated NDs were investigated. The dynamics results clearly exhibit slower relaxation in passivated NDs when compared to un-passivated NDs, and this can explain the difference in their luminescence intensities.

## Methods

The custom-built laser ablation equipment is shown in Fig. 1. The femtosecond laser (Light-Conversion Pharos, 343 nm,  $\sim 300$  fs, 90 kHz,  $9.2 \mu\text{J}\cdot\text{pulse}^{-1}$ ) first passed through aperture A1, then the beam expander (L1 and L2), and finally the galvanometer system (Sunny Technology, TSH8720M) composed of a F-theta system and field mirror aided by all-reflection mirror M1. Through the field mirror ( $f = 10$  cm), the laser was focused on the solid-liquid interface of bulk diamond (2 mm in diameter, 1 mm in thickness) in a quartz cuvette (optical length = 10 mm) filled with ethanol. The focus scanned on the target in concentric circles  $1 \mu\text{m}$  apart. After an hour, the colloid was collected and ultrasonicated for 45 min. Subsequently, the sample was divided into two parts wherein one was investigated without any

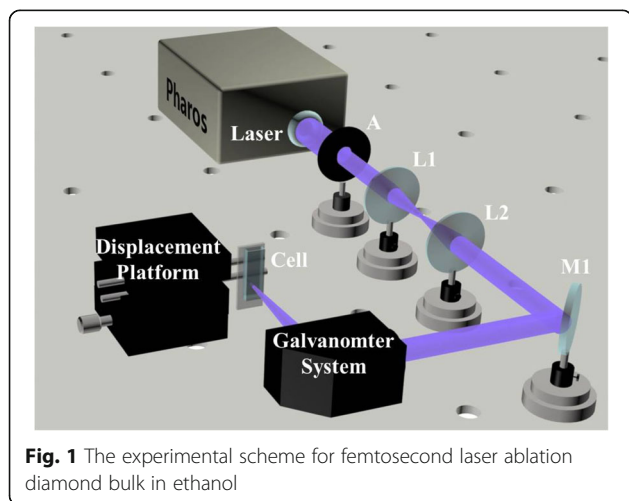


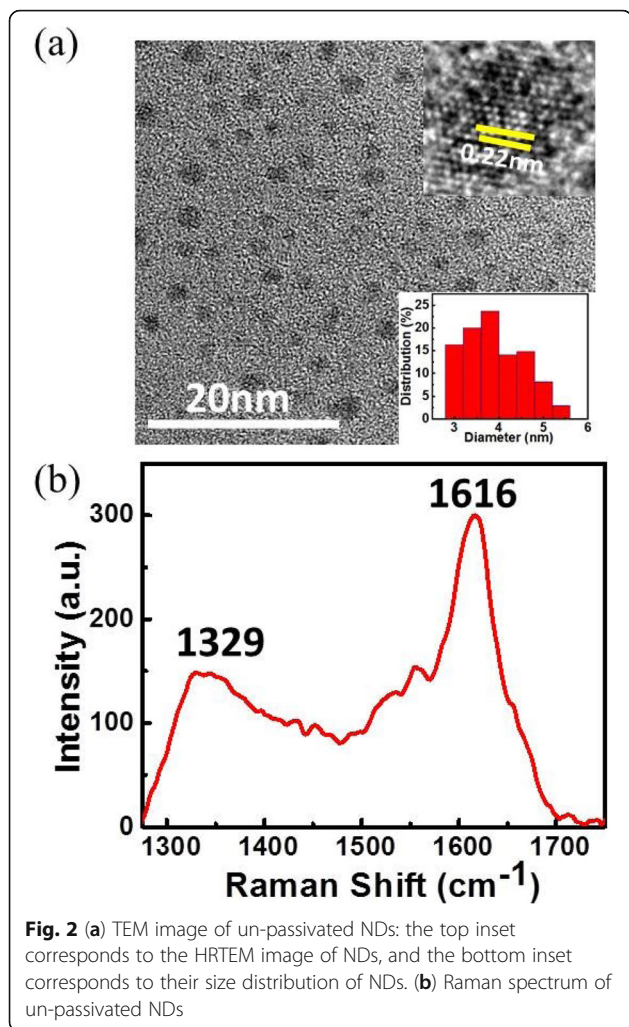
**Fig. 1** The experimental scheme for femtosecond laser ablation diamond bulk in ethanol

treatment (termed as un-passivated NDs) and the other after surface passivation (termed as passivated NDs). For surface passivation, 0.1 ml PEG<sub>400N</sub> (Sigma Aldrich, CAS: 25322-68-3) was dropped into a sample, and the mixture was subjected to ultrasonic treatment for 30 min, and then poured into the reactor. Finally, the reactor was maintained at  $120^\circ\text{C}$  for 72 h in an incubator.

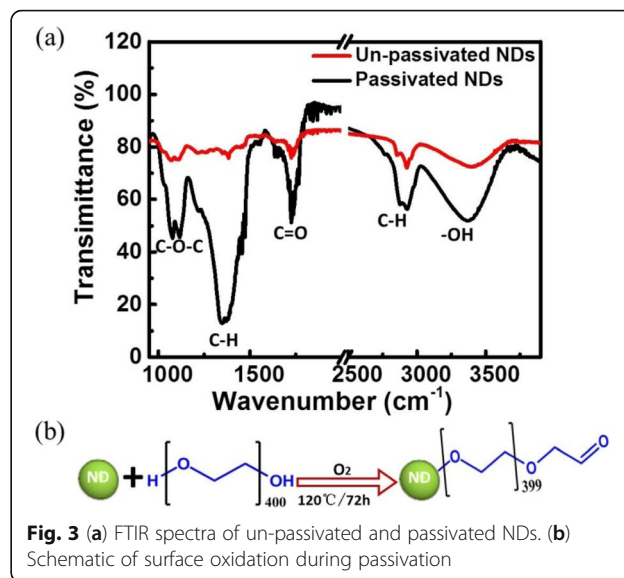
The morphology of NDs was characterized via a transmission electron microscope (TEM) and high-resolution transmission electron microscope (HRTEM) on the JEOL JEM-2100F. The size distribution was analyzed by the Nano Measurer software. Raman spectroscopy and Fourier transform infrared spectroscopy (FTIR) were performed to confirm the phase structure and surface ligands of NDs, respectively. Specifically, ultraviolet-visible (UV-Vis) absorption spectra and luminescence spectra were obtained to investigate the optical properties. The details of all the characterization equipment have been introduced in a previous study [24]. Time-resolved spectra were obtained using a fluorescence transient spectrometer (HORIBA, IHR320, 55ps) with a 390-nm NanoLED source (N-390).

## Results and Discussion

The morphology, size distribution, and lattice structure of un-passivated NDs are shown in Fig. 2a. It can be seen from the TEM image that the prepared ND particles are well-dispersed, and their shape is almost spherical. The inset HRTEM image in Fig. 2a shows that the spacing of the crystal face is approximately 0.22 nm which corresponds to the (111) plane of a diamond. The size analysis is based on 100 particles, as shown in the inset of Fig. 2a, and the average size of NDs is approximately 3.8 nm. Raman spectroscopy was performed to further prove that the sample exhibits a diamond phase. As shown in Fig. 2b, two peaks are located at  $1329 \text{ cm}^{-1}$  and  $1616 \text{ cm}^{-1}$  and are labeled peak D and peak G, respectively. Peak D originates from the zone center mode of  $T_{2g}$  symmetry of  $\text{sp}^3$  fraction [25]. Peak G is the zone center mode of  $E_{2g}$  symmetry of  $\text{sp}^2$  fraction [26, 27], and this indicates that defects exist in the NDs. When compared with the intrinsic peak of a diamond at  $1330 \text{ cm}^{-1}$ , peak D downshifts and broadens. This is because the size of NDs is smaller than the Bohr radius of diamond (6 nm) [28], which results in a quantum confinement effect [29]. As shown by Raman results, the intensity of peak G is stronger than that of peak D. However, the scattering cross-section of  $\text{sp}^2$  is 50–230 times larger than that of  $\text{sp}^3$ , and thus, the Raman scattering of  $\text{sp}^2$  is significantly more sensitive than that of  $\text{sp}^3$  [30]. Therefore, it can be concluded that most of the products are NDs by considering the results of TEM and Raman scattering.

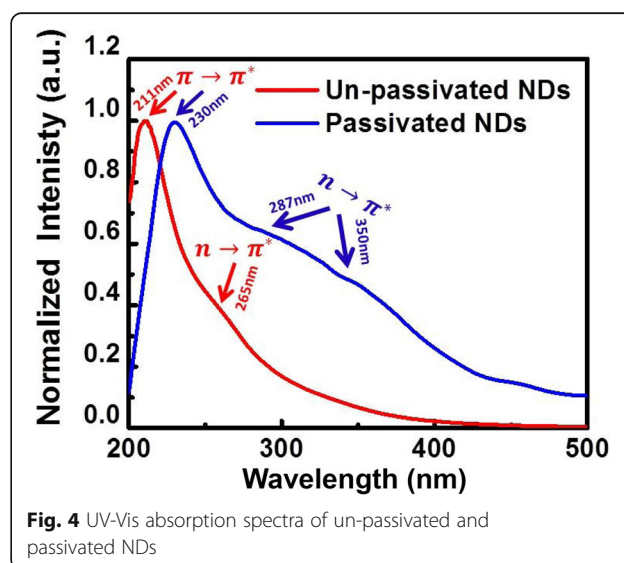


In order to investigate NDs' surfaces, FTIR spectra were studied. As shown in Fig. 3a, for either un-passivated or passivated NDs, the spectra exhibit a strong and broad peak at  $3380\text{ cm}^{-1}$  that is caused by stretching vibration of  $-\text{OH}$  bonds. The absorption peaks located between  $2800$  and  $3000\text{ cm}^{-1}$  originate from the stretching vibration of  $\text{C}-\text{H}$  bonds while the  $1380\text{ cm}^{-1}$  peak is due to the in-plane bending vibration of  $\text{C}-\text{H}$  bonds [31]. Given that NDs are prepared in ethanol, some  $-\text{OH}$  and  $-\text{CH}_x$  bonds are adsorbed on the surface of NDs during the preparation process. Additionally, certain oxidation results from the presence of oxygen in the ethanol solution, thereby resulting in a small amount of  $\text{C}=\text{O}$  and  $\text{C}-\text{O}-\text{C}$  bonds generated on the surface of un-passivated NDs, and this is clearly observed in the spectrum. One of the bonds is located at  $1726\text{ cm}^{-1}$  and is induced by the stretching vibration of  $\text{C}=\text{O}$  bonds [20]. The other bonds correspond to a symmetric bimodal at  $1074\text{ cm}^{-1}$  and  $1113\text{ cm}^{-1}$ , which originate from the  $\text{C}-\text{O}-\text{C}$  bonds [32]. However, after



passivation by  $\text{PEG}_{400\text{N}}$ , the intensity of all absorption peaks increases considerably. In addition to the massive introduction of  $\text{C}-\text{H}$  and  $-\text{OH}$  bonds, the oxidation degree significantly improved, which implies that a large number of the  $\text{C}=\text{O}$  and  $\text{C}-\text{O}-\text{C}$  bonds are formed on the passivated NDs' surface. At  $120\text{ }^\circ\text{C}$ , high pressure is formed inside the reactor with ethanol. Given the presence of oxygen, the hydroxyl groups on the surface of NDs are oxidized to form  $\text{C}=\text{O}$  and  $\text{C}-\text{O}-\text{C}$  bonds, as shown in Fig. 3b. Therefore, it is proven that NDs are successfully passivated by  $\text{PEG}_{400\text{N}}$ .

Figure 4 shows the UV-Vis absorption spectra of un-passivated and passivated NDs. The absorption spectra of un-passivated NDs exhibit a steep peak at  $211\text{ nm}$  originating from  $\pi \rightarrow \pi^*$  transition of  $\text{C}=\text{C}$  bonds and a shoulder at around  $265\text{ nm}$  originating from  $n \rightarrow \pi^*$



transition of C=O bonds of NDs [33]. Compared with un-passivated NDs, the passivated NDs display a shift in  $\pi \rightarrow \pi^*$  transition to 230 nm, and the 19-nm redshift is potentially due to the narrowing of NDs' bandwidth given the quantum confinement effect [34], which is induced by the increase in size after passivation [35]. Furthermore, the passivated NDs exhibit two shoulders at 287 nm and 350 nm both from  $n \rightarrow \pi^*$  transition and significantly exceed that of un-passivated NDs. The evident  $\pi \rightarrow \pi^*$  and  $n \rightarrow \pi^*$  transitions indicate that there are highly localized  $\pi$  states, and different trapping states are formed due to defects caused by surface oxidation.

The luminescence spectra of NDs are shown in Fig. 5. Figure 5a shows un-passivated NDs' maximal luminescence at 440 nm and 447 nm, which are nearly equal under 360 nm or 380 nm excitation. For passivated NDs, the maximal luminescence peak at 440 nm is excited by 380 nm wavelength, as shown in Fig. 5b. After comparison, the results indicate that under the same conditions, the luminescence peak positions of un-passivated and passivated NDs are almost unanimously dependent on the excitation wavelengths. When the excitation wavelength changes from 280 to 420 nm, the luminescence peaks redshift from 380 to 495 nm as shown in Fig. 5c.

As shown in Fig. 5d, the luminescence intensity increases and then decreases with increasing excitation wavelength for either sample. The difference is that the intensity of passivated NDs always exceeds that of un-passivated NDs. The ratio of luminescence peak intensity ( $I_{\text{passivated}}/I_{\text{un-passivated}}$ ) reaches 10 when excited at 380 nm. As shown in Fig. 5e, the full width at half maximum (FWHM) of the luminescence displays an overall decreasing trend, and the trend is almost consistent for both samples when the excitation wavelength is less than 360 nm. The FWHM began to diverge when the excitation wavelength corresponds to 380 nm. For un-passivated NDs, their FWHM gradually decreases, and it reaches a minimum of 63 nm for passivated NDs when the excitation wavelength is 380 nm. As shown in Fig. 5d, the enhancement due to surface passivation is not equal and it reaches the maximum with excitation at 380 nm, and the reason may be surface passivation makes NDs distribute more uniformly, thereby FWHM decreases. Thus, the FWHM relatively increases due to more discrete NDs' luminescence with excitation at 400 nm and 420 nm.

In order to investigate the luminescence mechanism of NDs with different surface states, transient-state spectra

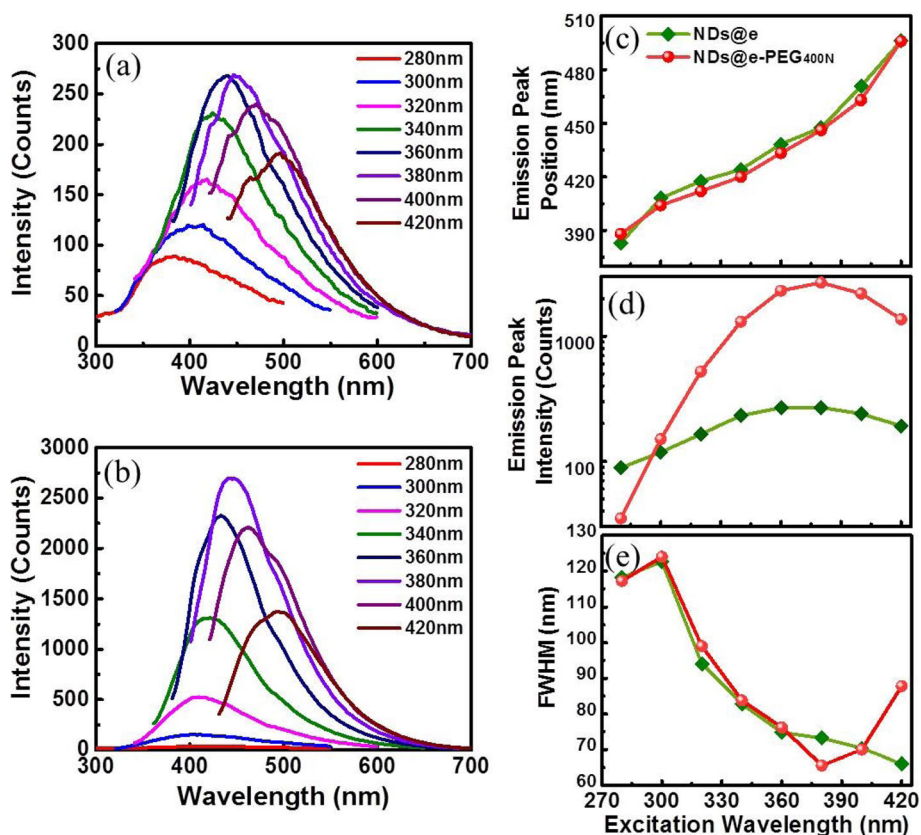


**Fig. 5** Luminescence spectra of un-passivated (a) and passivated (b) NDs excited at 280–420 nm. The change in luminescence peak wavelengths (c), luminescence peak intensity (d), and FWHM (e) are various with the excitation wavelength

are obtained using the time-resolved method, and the decay curves are shown in Fig. 6a, b. Evidently, the luminescence decay rate of un-passivated NDs is faster than that of passivated NDs. The decay curves are fitted with three exponential functions and tabulated in Table 1. At 420 nm and 440 nm, decay data can be well fitted with components  $\tau_1$  and  $\tau_2$ . At 480 nm and 520 nm, they can be well fitted with three components  $\tau_1$ ,  $\tau_2$ , and  $\tau_3$ . Specifically,  $\tau_1$  (1.00–1.91 ns) corresponds to the fast component, which is correlated with the non-radiative recombination of electron trapping during transition. Furthermore,  $\tau_2$  (5.51–6.41 ns) and  $\tau_3$  (16.3–32.8 ns) correspond to slow components, which are mainly derived from radiative recombination. Additionally,  $\tau_2$  corresponds to the lifetime of radiative combination from trapping states to the localized  $\pi$  state, and it remains almost unchanged at 5.51–6.41 ns for NDs. Moreover,  $\tau_3$  is attributed to the electron's radiative transition from a molecule-like cluster [36].

For un-passivated NDs,  $\tau_1$  (1.00 ns) accounts for 83.2% at 420 nm. When the luminescence wavelength increases to 520 nm,  $\tau_1$  reaches to 1.62 ns while the proportion decreases to 65.7%. The reason is attributed to the increased deviation between the trapping state and excited state at the band edge. The  $\tau_2$  component is maintained at approximately 6.0 ns, although its proportion increased from 16.8% (420 nm) to 33.7% (520 nm). It should be noted that at 480 nm and 520 nm, slow component  $\tau_3$  is present, but the proportion is less than 1%.

For passivated NDs, the longest  $\tau_1$  and  $\tau_2$  appear at the strongest luminescence at 440 nm and correspond to 1.91 ns and 6.41 ns, respectively. The lifetimes of both components decrease when the luminescence peak moves toward the band edge. The contribution of fast component  $\tau_1$  gradually decreases from 70.6 to 52.2%, the slow component  $\tau_2$  increases from 29.4 to 44.1%, and  $\tau_3$  increases from 2.6 to 3.7%. It is worth noting that the fast component is the main contributor to the luminescence lifetime of NDs.

The proportions of lifetimes  $\tau_1$  and  $\tau_2$  for un-passivated and passivated NDs are shown in Fig. 6c. Generally, the fast component  $\tau_1$  exhibits an overall decrease after NDs are passivated while slow components  $\tau_2$  and  $\tau_3$  display opposite trends. This is because the trapping states are modified, which leads to more possibilities for radiative combination from trapping states to  $\pi$  state. Inevitably, the decrease in the fast component and the increase in slow components increase the average lifetime of passivated NDs as shown in Fig. 6d. Hence, the luminescence decay rate of passivated NDs is slower than that of un-passivated NDs. Furthermore, for either un-passivated or passivated NDs, the average lifetime gets longer with increases in luminescence wavelength. Electrons tend to transfer from trapping states with lower energy levels to the  $\pi$  state to realize radiative recombination, and thus, more slow components contribute to the lifetime of longer luminescence wavelengths.

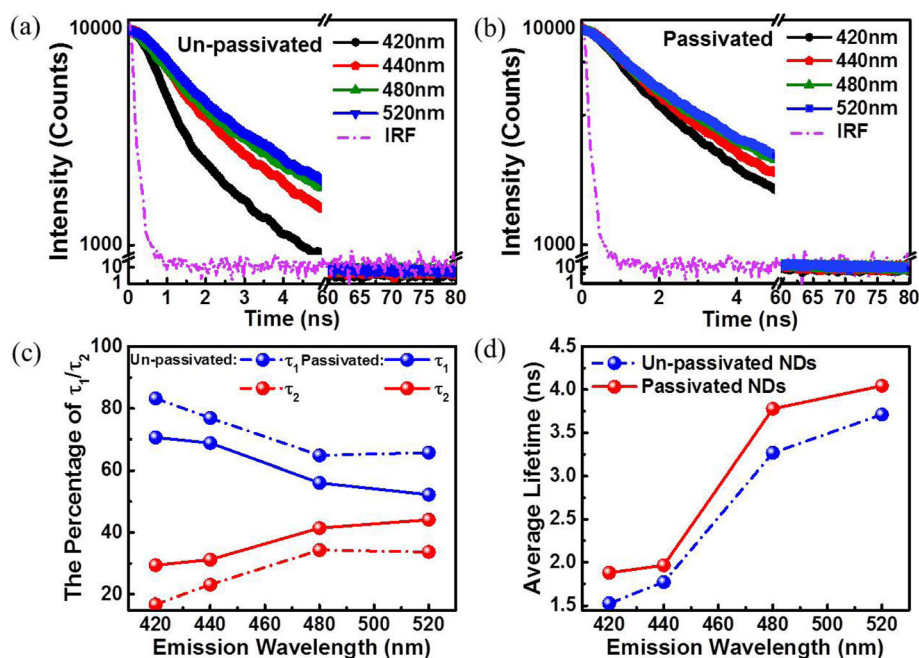


**Fig. 6** Time-resolved luminescence of un-passivated (a) and passivated (b) NDs at different luminescence wavelengths. (c) Percentage of  $\tau_1$  and  $\tau_2$  changes at different luminescence wavelengths. (d) Average lifetime of different luminescence wavelength for passivated and un-passivated NDs

**Table 1** Lifetimes ( $\tau_1$ ,  $\tau_2$ , and  $\tau_3$ ) and relative contributions for un-passivated and passivated NDs at 390 nm excitation

	$\lambda_{Em}$ (nm)	$\tau_1$ (ns)	$\tau_1$ (%)	$\tau_2$ (ns)	$\tau_2$ (%)	$\tau_3$ (ns)	$\tau_3$ (%)
Un-passivated NDs	420	1.00	83.2	5.51	16.8	–	–
	440	1.49	76.9	6.15	23.1	–	–
	480	1.50	64.8	5.64	34.3	23.0	0.9
	520	1.62	65.7	6.03	33.7	32.8	0.6
Passivated NDs	420	1.71	70.6	5.82	29.4	–	–
	440	1.91	68.8	6.41	31.2	–	–
	480	1.83	56.0	5.88	41.4	17.6	2.6
	520	1.75	52.2	5.86	44.1	16.3	3.7

## Conclusions

In conclusion, well-dispersed NDs with dominant  $sp^3$  phase and an average size of 3.8 nm were successfully prepared in this study. The NDs are passivated by PEG<sub>400N</sub> for future applications. After passivation, three absorption bands appeared in the absorption spectra. One of the bands is located at 230 nm originating from  $\pi \rightarrow \pi^*$  transition and displays a 19-nm redshift when compared with un-passivated NDs. The luminescence peaks of NDs were almost unchanged with or without passivation, and NDs emit significantly blue luminescence at 440 nm after passivation. Based on time-resolved luminescence analysis, passivated NDs decay slower than un-passivated NDs. This is due to the increased proportion of radiative combination from trapping states to localized  $\pi$  states transition due to surface modification. The results indicate that passivation does not destroy the structure of NDs, and instead improves their luminescence intensity as high as 10 times and prolongs the lifetime, which is very important for application in target tracking and localization in vivo.

## Abbreviations

NDs: Nano-diamonds; fs-PLAL: Femtosecond pulsed laser ablation in liquid; FTIR: Fourier transform infrared spectroscopy; UV-Vis: Ultraviolet-visible; FWHM: Full width at half maximum; TEM: Transmission electron microscope; HRTEM: High-resolution transmission electron microscope; PEG<sub>400N</sub>: Polyethylene glycol-400N

## Acknowledgements

The authors thank Chao Lv in the State Key Laboratory of Integrated Optoelectronics for the help in TEM tests.

## Authors' Contributions

JH and LYP prepared NDs with and without PEG<sub>400N</sub> passivation experiments; carried out the UV-Vis absorption, FTIR, and steady-state luminescence spectra; and wrote the manuscript. MHA performed the transient fluorescence spectra tests. YZD drew the chemical reaction mechanism involved in the surface passivation. BRG managed the checking and revising of the manuscript. All authors read and approved the final manuscript.

## Funding

This work is supported by the National Key Research and Development Program of China (No. 2017YFB1104600) and the National Natural Science Foundation of China (NSFC) (No. 61825502, 61590930, 61827826, 21903035, 61575079).

## Availability of Data and Materials

The authors declare that the materials, data, and associated protocols are available to the readers.

## Competing Interests

The authors declare that they have no competing interests.

Received: 18 December 2019 Accepted: 3 August 2020

Published online: 20 August 2020

## References

- Samuel MS, Shah SS, Bhattacharya J et al (2018) Adsorption of Pb(II) from aqueous solution using a magnetic chitosan/graphene oxide composite and its toxicity studies. *Int J Biol Macromol* 115:1142–1150
- Samuel MS, Shah SS, Subramanian V et al (2018) Preparation of graphene oxide/chitosan/ferrite nanocomposite for chromium(VI) removal from aqueous solution. *Int J Biol Macromol* 119:540–547
- Hsu PC, Chang HT (2012) Synthesis of high-quality carbon nanodots from hydrophilic compounds: role of functional group. *Chem Commun* 48:3984–3986
- Mostofizadeh A, Li Y, Song B et al (2011) Synthesis, properties, and applications of low-dimensional carbon-related nanomaterials. *J Nanomater* 2011:1–21
- Yi H, Huang D, Qin L et al (2018) Selective prepared carbon nanomaterials for advanced photocatalytic application in environmental pollutant treatment and hydrogen production. *Appl Catal B Environ* 239:408–424
- Yamashita T, Yamashita K, Nabeshi H et al (2012) Carbon nanomaterials: efficacy and safety for nanomedicine. *Materials (Basel)* 5(2):350–363
- Mochalin VN, Shenderova O, Ho D, Gogotsi Y (2011) The properties and applications of nanodiamonds. *Nat Nanotechnol* 7(1):11–23
- Kurantowicz N, Strojny B, Sawosz E, Jaworski S et al (2015) Biodistribution of a high dose of diamond, graphite, and graphene oxide nanoparticles after multiple intraperitoneal injections in rats. *Nanoscale Res Lett* 10(1):398
- Zimmermann T, Kubovic M, Denisenko A, Janischowsky K et al (2005) Ultra-nano-crystalline/single crystal diamond heterostructure diode. *Diam Relat Mater* 14(3-7):416–420
- Wang X, Low XC, Hou WX, Abdullah LN et al (2014) Epirubicin-adsorbed nanodiamonds kill chemoresistant hepatic cancer stem cells. *ACS Nano* 8(12):12151–12166
- Zhang XQ, Chen M, Lam R, Xu XY et al (2009) Polymer-functionalized nanodiamond platforms as vehicles for gene delivery. *ACS Nano* 3(9):2609–2616
- Cheng XB, Zhao MQ, Chen C, Pentecost A et al (2017) Nanodiamonds suppress the growth of lithium dendrites. *Nat Commun* 8(1):336
- Krüger A, Kataoka F, Ozawa M, Fujino T et al (2005) Unusually tight aggregation in detonation nanodiamond: identification and disintegration. *Carbon* 43(8):1722–1730
- Xu K, Xue QJ (2007) Deaggregation of ultradispersed diamond from explosive detonation by a graphitization-oxidation method and by hydroiodic acid treatment. *Diam Relat Mater* 16(2):277–282
- Kumar A, Ann Lin P, Xue A, Hao B et al (2013) Formation of nanodiamonds at near-ambient conditions via microplasma dissociation of ethanol vapour. *Nat Commun* 4:2618

16. Naragino H, Tominaga A, Hanada K, Yoshitake T (2015) Synthesis method for ultrananocrystalline diamond in powder employing a coaxial arc plasma gun. *Appl Phys Express* 8(7):075101
17. Tan DZ, Zhou SF, Xu BB, Chen P et al (2013) Simple synthesis of ultra-small nanodiamonds with tunable size and photoluminescence. *Carbon* 62:374–381
18. Nakahara S, Stauss S, Miyazoe H, Shizuno T et al (2010) Pulsed laser ablation synthesis of diamond molecules in supercritical fluids. *Appl Phys Express* 3(9):096201
19. Tan DZ, Yamada Y, Zhou S, Shimotsuna Y et al (2014) Carbon nanodots with strong nonlinear optical response. *Carbon* 69:638–640
20. Ray SC, Saha A, Jana NR, Sarkar R (2009) Fluorescent carbon nanoparticles: synthesis, characterization, and bioimaging application. *J Phys Chem C* 113: 18546–18551
21. Gur FN, McPolin CPT, Raza S, Mayer M et al (2018) DNA-assembled plasmonic waveguides for nanoscale light propagation to a fluorescent nanodiamond. *Nano Lett* 18(11):7323–7329
22. Shenderova OA, Shames AI, Nunn NA, Torelli MD et al (2019) Review article: synthesis, properties, and applications of fluorescent diamond particles. *J Vac Sci Technol B Nanotechnol Microelectron* 37(3):030802
23. Su LX, Lou Q, Jiao Z, Shan CX (2016) Plant cell imaging based on nanodiamonds with excitation-dependent fluorescence. *Nanoscale Res Lett* 11(1):425
24. Hao J, Pan LY, Gao S, Fan H et al (2019) Production of fluorescent nanodiamonds through femtosecond pulsed laser ablation. *Optical Materials Express* 9(12):4734
25. Ferrari AC, Robertson J (2000) Interpretation of Raman spectra of disordered and amorphous carbon. *Phys Rev B* 61(20):14095–14107
26. Nemanich RJ, Solin SA (1979) First- and second-order Raman scattering from finite-size crystals of graphite. *Phys Rev B* 20(2):392–401
27. Tan DZ, Yamada Y, Zhou S, Shimotsuna Y et al (2013) Photoinduced luminescent carbon nanostructures with ultra-broadly tailored size ranges. *Nanoscale* 5(24):12092–12097
28. Gheeraert E, Kozumi S, Teraji T, Kanda H et al (1999) Electronic states of boron and phosphorus in diamond. *Phys Status Solidi A* 174(1):39–51
29. Tae EL, Lee KE, Jeong JS, Yoon KB (2008) Synthesis of diamond-shape titanate molecular sheets with different sizes and realization of quantum confinement effect during dimensionality reduction from two to zero. *J Am Chem Soc* 130(20):6534–6543
30. Robertson J (2002) Diamond-like amorphous carbon. *Mater Sci Eng R* 37: 129–281
31. Osswald S, Yushin G, Mochalin V, O S et al (2006) Control of sp<sup>2</sup>/sp<sup>3</sup> carbon ratio and surface chemistry of nanodiamond powders by selective oxidation in air. *JACS* 128:11635–11642
32. Srivastava S, Gajbhiye NS (2011) Carbogenic nanodots: photoluminescence and room-temperature ferromagnetism. *Chemphyschem* 12(14):2624–2632
33. Eda G, Lin YY, Mattevi C, Yamaguchi H et al (2010) Blue photoluminescence from chemically derived graphene oxide. *Adv Mater* 22(4):505
34. Holt KB (2010) Undoped diamond nanoparticles: origins of surface redox chemistry. *Phys Chem Chem Phys* 12(9):2048–2058
35. Jungnickel G, Frauenheim T, Porezag D, Blaudeck P et al (1994) Structural properties of amorphous hydrogenated carbon. IV. A molecular-dynamics investigation and comparison to experiments. *Phys Rev B Condens Matter* 50(10):6709–6716
36. Galande C, Mohite AD, Naumov AV, Gao W et al (2011) Quasi-molecular fluorescence from graphene oxide. *Sci Rep* 1:85

## Publisher's Note

Springer Nature remains neutral with regard to jurisdictional claims in published maps and institutional affiliations.

Submit your manuscript to a SpringerOpen<sup>®</sup> journal and benefit from:

- Convenient online submission
- Rigorous peer review
- Open access: articles freely available online
- High visibility within the field
- Retaining the copyright to your article

---

Submit your next manuscript at ► [springeropen.com](https://www.springeropen.com)

---